A Discrete BCG-FFT Algorithm for Solving 3D Inhomogeneous Scatterer Problems [1]

HONG GAN AND WENG CHO CHEW

ELECTROMAGNETICS LABORATORY
DEPARTMENT OF ELECTRICAL AND COMPUTER ENGINEERING
UNIVERSITY OF ILLINOIS
URBANA, IL 61801

Abstract

In this paper, an algorithm for computation of the scattered fields from three dimensional inhomogeneous dielectric scatterers is presented. In this method, the Galerkin's testing formulation of an integral equation for 3D electromagnetic (EM) fields is represented by a multi-input and multi-output linear system with known kernels. On a regular grid with rooftop basis functions, the kernels are discretized and accurately evaluated. Furthermore they are represented by Toeplitz matrices which dramatically reduces the storage and computational complexity in solving for the scattered fields. Also, the kernels are independent of the scattering configuration and the incident waves. For a given frequency, they can be evaluated once and for all. The biconjugate gradient (BCG) algorithm combined with fast Fourier transform (FFT) is applied to solve the discrete linear system iteratively. The memory required for this algorithm is of order N, and the computational complexity of the BCG process costs order $N \log N$ operations per iteration, where N is the number of 3D unknowns. Unlike previous approaches, no approximation is made when FFT is used to accelerate the matrix-vector multiplication.

[1]This work is supported by NSF under contract NSF-ECS-92-24466, ARO under contract DAAL03-91-G-0339, and ONR under contract N00014-89-J-1286. December. 5, 1994

1 Introduction

Modeling and efficient computation of scattered fields from arbitrary scatterers in a three dimensional (3D) space play an important role in both forward scattering analyses and inverse scattering problems, which have many applications in communication, target identification, nondestructive testing, geophysical exploration, and microwave imaging.

When the support of the scatterer is bounded, the integral equation of the scattered fields accounts for the radiation boundary condition, and limits the solution domain only over the support of the scatterer. For this reason, numerical techniques to solve the integral equation using the method of moments (MOM) have been studied in many applications [1]-[3]. In MOM, the integral equation of the scattered field [4] is discretized and represented by a set of linear algebraic equations. Then numerical methods are used to solve the equations. Today, commonly applied algorithms for this purpose are based on conjugate gradient (CG) type methods [5, 6] which search for the solution iteratively. However, a serious drawback of the method is that the integral formulation results in a dense matrix formulation. The computational resources required in practice, such as the storage and CPU time, have limited its applications, and considerable research efforts have been undertaken to overcome these difficulties, such as the fast recursive algorithms [7], the conjugate gradient and fast Fourier transform (CG-FFT) [8]-[10], and the use of wavelet expansion approaches [11, 12].

Based on the convolutional relationship between the source and the dyadic Green function in the integral equation, a commonly suggested approach is a CG-FFT type algorithm which uses FFT algorithm to implement the convolution between the Green's function and the equivalent current. For planar or two dimensional problems, the application of CG-FFT technique can be found in [13]-[17]. Liu and Chew [18] extended this idea to axisymmetric problems using the fast Fourier-Hankel transforms (FFHT) instead of the FFT.

At present for three dimensional electrodynamic problems, there are two types of CG-FFT algorithms corresponding to their different ways of treating the singularity and the differential operators in the dyadic Green function. One is the point collocation method [8, 9], where the differential operators are approximated numerically using a finite difference formulation. The second method, the weak formulation [10], may be considered as a modification of the point collocation method, whereby the testing formulation is obtained by averaging the fields over each element. By doing so, the singularity of the Green's function is avoided and the second order derivatives are reduced to the first order derivatives.

We refer to those approaches discussed above as continuous CG-FFT methods since the

FFT is applied directly to the Green's function and the equivalent current. As a result, the dimension of the FFT has to be larger than the actual number of unknowns to achieve satisfactory accuracy, since the sampling rate for both equivalent current and the Green's function has to be larger due to the singularity of the Green's function and the Nyquist sampling rate. Another shortcoming of the continuous methods is that it is difficult to evaluate the conjugate transpose of the matrix based on the continuous formulation. Consequently, the choice of iterative solvers is limited.

In this paper, we present a discrete formulation for solving the 3D scattering problems. The scattered fields from dielectric scatterers with arbitrary geometry are modeled using integral equation with equivalent sources. The inhomogeneity of the parameter of the scatterer is approximated by a set of 3D simple functions. The total field is represented by a set of local basis functions. Flux continuity is enforced over all interfaces of the elements. A Galerkin's testing formulation is applied and no approximation is made to the differential operators involved in the integral equation except for the projection of the unknown field and the operators onto the subspace spanned by the basis functions.

It will be shown that the testing formulation can be represented by a multi-input and multi-output system with known linear kernels. The kernels are discretized using the rooftop basis functions and they are independent of the scattering configuration and the incident waves. Consequently, for a given sampling rate per wavelength, one need only evaluate once the kernels whose storage is of order N. This property is of particular interests for solving inverse problems. The problem of solving the integral equation is equivalent to the deconvolution problem where the unknown fields inside the scatterers are modulated with the dielectric permittivity distribution.

It will also be seen that by applying the Galerkin's testing formulation, the two gradient operators included in the dyadic Green's function are moved to the testing functions and the equivalent current. As a results, the discrete model developed here accurately represents the testing formulation of the integral equation. Meanwhile, the singularity in the Green's function is two orders lower than the point collocation method used in the schemes of Catedra *et al.*[8] and Shen *et al.* [9]. Moreover, differing from the weak form of CG-FFT by Zwamborn and Berg [10], the approach we proposed here makes no approximation when BCG-FFT is applied to solve the MOM matrix equation. The singularity of the Green's function in the volume integration is integrable for the evaluation of the matrix elements. Hence, the spherical mean approximation used in [10], which makes the testing formulation weaker, is avoided.

The biconjugate gradient (BCG) algorithm [5] combined with fast Fourier transform

(FFT) [19, 20] is applied to solve for the unknown field iteratively. The discrete model we have developed here is more efficient for the FFT operation since the kernels are finite discrete sequences. Therefore one need not enlarge the dimension of the FFT. Furthermore, the operation of the conjugate transpose of the matrix with a vector can also be conveniently implemented using FFT. Consequently, efficient techniques for solving linear algebraic equations requiring the conjugate transpose of a matrix [5], such as BCG approach, can be employed to solve the problem without increasing the computational complexity and the condition number. BCG generally requires a smaller number of iteration for convergence compared to CG on the normal equation.

To illustrate the use of this method, the total electric field and the bistatic radar cross sections (RCS) of several homogeneous and inhomogeneous spherical objects are computed. The computed results are verified by comparison with results obtained from Mie series solutions. The simulation results illustrate that with the discrete model, one can study 3D vector field using limited computer resources, such as workstation type computers, with satisfactory accuracy.

The organization of this paper is as follows: In Section 2, the Galerkin's testing formulation for solving the 3D integral equation of electromagnetic fields is formulated. In Section 3, a discrete linear system for the 3D electromagnetic scattering field is developed. Then the derivation of the linear kernels and the summary of the BCG-FFT algorithm are presented. Some numerical simulation results and the comparison with analytical solutions are presented in Section 4. Finally, the conclusions are given in Section 5.

2 Description of the Scattered Fields

2.1 Governing Equation

We consider scattered fields generated by an inhomogeneous scatterer illuminated by a given incident wave $\mathbf{E}_{inc}$. The scatterer is described by the distribution function $O(\mathbf{r})$ defined as the difference between the dielectric permittivity $\epsilon(\mathbf{r})$ of the scatterer and the dielectric permittivity ϵ_0 of the background medium and normalized to ϵ_0 :

$$O(\mathbf{r}) = \frac{\epsilon - \epsilon_0}{\epsilon_0} \tag{1}$$

The total electric field can be described by the integral equation [4]:

$$\mathbf{E}(\mathbf{r}) = \mathbf{E}_{inc}(\mathbf{r}) + k_0^2 \int_V \bar{\mathbf{G}}(\mathbf{r}, \mathbf{r}') \cdot O(\mathbf{r}')\mathbf{E}(\mathbf{r}')d^3r' \tag{2}$$

where $\bar{\mathbf{G}}$ is the dyadic Green's function defined as:

$$\bar{\mathbf{G}}(\mathbf{r},\mathbf{r}') = \left(\bar{\mathbf{I}} + \frac{\nabla\nabla}{k_0^2}\right) g(\mathbf{r},\mathbf{r}') \tag{3}$$

$$g(\mathbf{r},\mathbf{r}') = \frac{e^{ik|\mathbf{r}-\mathbf{r}'|}}{4\pi|\mathbf{r}-\mathbf{r}'|} \tag{4}$$

where $\mathbf{r}$ is the observation location, $\mathbf{r}'$ represents the source location, and V is the support of the function $O(\mathbf{r})$.

The scattered field is defined as the difference between the total field and the incident field:

$$\mathbf{E}_s(\mathbf{r}) = \mathbf{E}(\mathbf{r}) - \mathbf{E}_{inc}(\mathbf{r}) \tag{5}$$

Hence, the scattered field can be written as:

$$\mathbf{E}_s(\mathbf{r}) = k_0^2 \int_V \bar{\mathbf{G}}(\mathbf{r},\mathbf{r}') \cdot O(\mathbf{r}')\mathbf{E}(\mathbf{r}')d^3r' \tag{6}$$

It can be further represented explicitly in terms of the scalar Green's function:

$$\mathbf{E}_s(\mathbf{r}) = k_0^2 \int_V g(\mathbf{r},\mathbf{r}')O(\mathbf{r}')\mathbf{E}(\mathbf{r}')d^3r' + \nabla \int_V g(\mathbf{r},\mathbf{r}')\nabla' \cdot (O(\mathbf{r}')\mathbf{E}(\mathbf{r}'))d^3r' \tag{7}$$

The forward scattering problem is to solve for the electric field over the support of the function O.

2.2 Galerkin's Testing Formulation

To simplify the imposing of the boundary condition, the electric displacement field $\mathbf{D}$ is chosen as the unknown field for dielectric scatterers. The integral equation for field $\mathbf{D}$ can be obtained directly from Equation (2):

$$\mathbf{E}_{inc}(\mathbf{r}) = \frac{1}{\epsilon(\mathbf{r})}\mathbf{D}(\mathbf{r}) - k_0^2 \int_V g(\mathbf{r},\mathbf{r}')\chi(\mathbf{r}')\mathbf{D}(\mathbf{r}')d^3r' - \nabla \int_V g(\mathbf{r},\mathbf{r}')\nabla' \cdot [\chi(\mathbf{r}')\mathbf{D}(\mathbf{r}')]d^3r' \tag{8}$$

where $\chi(\mathbf{r})$ is the relative distribution function defined as $\chi(\mathbf{r}) \equiv \frac{O(\mathbf{r})}{\epsilon(\mathbf{r})}$.

To solve the above integral equation numerically, first, the support of function O is divided into a number of cells whose sizes are small enough so that the unknown field can be approximated by a set of basis functions in each cell with satisfactory accuracy. By applying the flux continuity boundary conditions to the interfaces among the cells, one can write:

$$\mathbf{D}(\mathbf{r}) = \sum_n^{\infty} \mathbf{f}_n(\mathbf{r})d_n \approx \sum_n^{N} \mathbf{f}_n(\mathbf{r})d_n \tag{9}$$

where $\mathbf{f}_n$ are the vector basis functions with support V_n and finite divergence, N is the total number of basis functions, and the support of function O is covered by the union of the supports of all basis functions $V = \bigcup_{n=1}^{N} V_n$. The Galerkin's testing formulation for solving Equation (8) can be written as:

$$< \mathbf{f}_k, \mathbf{E}_{inc}(\mathbf{r}) >=< \mathbf{f}_k, \frac{1}{\epsilon(\mathbf{r})}\mathbf{D}(\mathbf{r}) > - < \mathbf{f}_k, \mathbf{E}_s(\mathbf{r}) > \tag{10}$$

where the scattered field $\mathbf{E}_s$ takes the form:

$$\mathbf{E}_s(\mathbf{r}) = k_0^2 \int_V g(\mathbf{r}, \mathbf{r}')\chi(\mathbf{r}')\mathbf{D}(\mathbf{r}')d^3r' + \nabla \int_V g(\mathbf{r}, \mathbf{r}')\nabla' \cdot [\chi(\mathbf{r}')\mathbf{D}(\mathbf{r}')]d^3r' \tag{11}$$

for $k, n = 1, 2, \cdots, N$. Here, $< \cdot, \cdot >$ denotes the integration of the inner product of two vector functions over the intersection of their supports.

Substituting the expansion for $\mathbf{D}$ into the above equation and moving the ∇ operator in the second term of the scattered field in Equation (11) to the testing function using integration by parts result in:

$$\begin{aligned} < \mathbf{f}_k, \mathbf{E}_{inc}(\mathbf{r}) > \;=\; & \sum_m \Big[< \mathbf{f}_k, \frac{1}{\epsilon(\mathbf{r})}\mathbf{f}_m > \\ & - < \mathbf{f}_k, k_0^2 \int_{V_m} g(\mathbf{r}, \mathbf{r}')\chi(\mathbf{r}')\mathbf{f}_m(\mathbf{r}')d^3r' > \\ & + < \nabla \cdot \mathbf{f}_k, \int_{V_m} g(\mathbf{r}, \mathbf{r}')\nabla' \cdot (\chi(\mathbf{r}')\mathbf{f}_m(\mathbf{r}'))d^3r' > \Big] d_m \end{aligned} \tag{12}$$

For brevity, denoting

$$b_k =< \mathbf{f}_k, \mathbf{E}_{inc}(\mathbf{r}) > \tag{13}$$

$$a_{k,m} =< \mathbf{f}_k, \frac{1}{\epsilon(\mathbf{r})}\mathbf{f}_m > \tag{14}$$

$$\begin{aligned} g_{k,m} = & - < \mathbf{f}_k, k_0^2 \int_{V_m} g(\mathbf{r}, \mathbf{r}')(\chi(\mathbf{r}')\mathbf{f}_m(\mathbf{r}')d^3r' > \\ & + < \nabla \cdot \mathbf{f}_k, \int_{V_m} g(\mathbf{r}, \mathbf{r}')\nabla \cdot (\chi(\mathbf{r}')\mathbf{f}_m(\mathbf{r}'))d^3r' > \end{aligned} \tag{15}$$

one can write Equation (12) as:

$$b_k = \sum_m^N (a_{k,m} - g_{k,m})d_m \tag{16}$$

for $k = 1, 2, \cdots, N$. Or in a more compact matrix notation, Equation (12) takes the form:

$$(\bar{\mathbf{A}} + \bar{\mathbf{G}}) \cdot \mathbf{d} = \mathbf{b} \tag{17}$$

where $\bar{\mathbf{A}} = \{a_{k,m}\}$, $\bar{\mathbf{G}} = \{g_{k,m}\}$, $\mathbf{d} = \{d_m\}$, and $\mathbf{b} = \{b_k\}$. The problem now is to solve the matrix equation (17) for the vector $\mathbf{d}$. Once $\mathbf{d}$ is obtained, one can evaluate the scattered field at any interested location using Equation (2).

3 Discrete Linear System Structure

In the above matrix equation, the matrix $\bar{\mathbf{A}}$ is a band-limited sparse matrix. However, the matrix $\bar{\mathbf{G}}$ is a dense matrix. Directly storing and evaluating $\bar{\mathbf{G}}$ and solving for the field $\mathbf{d}$ are very expensive. Therefore, further simplification of Equation (17) is required.

3.1 Discretization of the Field Using Face Based Elements

We choose cuboid as the support of a basic element. The center of an element is located at (x_i, y_j, z_k) on Cartesian coordinates. Here, i, j, and k represent the discrete indices of x, y, and z coordinates, respectively. A 3D cuboid pulse function is defined as:

$$P_{ijk}(x,y,z) = T_i(x)T_j(y)T_k(z) \tag{18}$$

where $T_p(t), p = i, j, k$ is a one dimensional pulse function centered at p with support Δ_t. The rooftop function [8] is chosen as the basis. Then the basis functions for the $\hat{x}$ component of the flux can be written as:

$$\mathbf{f}^x_{ijk}(x,y,z) = \boldsymbol{\phi}^x_i P_{i,j,k}(x,y,z) + \boldsymbol{\psi}^x_{i+1} P_{i+1,j,k}(x,y,z). \tag{19}$$

Similarly, the basis functions for the $\hat{y}$ and $\hat{z}$ components take the form:

$$\mathbf{f}^y_{ijk}(x,y,z) = \boldsymbol{\phi}^y_j P_{i,j,k}(x,y,z) + \boldsymbol{\psi}^y_j P_{i,j+1,k}(x,y,z), \tag{20}$$

$$\mathbf{f}^z_{ijk}(x,y,z) = \boldsymbol{\phi}^z_k P_{i,j,k}(x,y,z) + \boldsymbol{\psi}^z_{k+1} P_{i,j,k+1}(x,y,z), \tag{21}$$

where

$$\begin{aligned}
\boldsymbol{\phi}^x_i &= \hat{x}\xi_i, \quad \boldsymbol{\psi}^x_i = \hat{x}(1-\xi_i), \\
\boldsymbol{\phi}^y_j &= \hat{y}\zeta_j, \quad \boldsymbol{\psi}^y_j = \hat{y}(1-\zeta_j), \\
\boldsymbol{\phi}^z_k &= \hat{z}\eta_k, \quad \boldsymbol{\psi}^z_k = \hat{z}(1-\eta_k),
\end{aligned}$$

$$\xi_i = \frac{x-x_i}{\Delta X_i} + \frac{1}{2}, \quad \zeta_j = \frac{y-y_j}{\Delta Y_j} + \frac{1}{2}, \quad \eta_k = \frac{z-z_k}{\Delta Z_k} + \frac{1}{2}.$$

The profiles of the basis functions with respect to the p^{th} coordinate are plotted in Figure 1.

Since the rooftop basis functions $\mathbf{f}^p_{ijk}(\mathbf{r}), p = x, y, z$ described above sample the p^{th} component of the field $\mathbf{D}$ on the center of interfaces of rectangular cells with normal pointing to the direction p, they are also referred to as face-based elements in 3D space.

For brevity, in the remainder of the text, the three-index notation is compressed into a vector index $\mathbf{m}$ which is defined as $\mathbf{m} \equiv m_x\hat{x} + m_y\hat{y} + m_z\hat{z}$. Here m_x, m_y and m_z are the

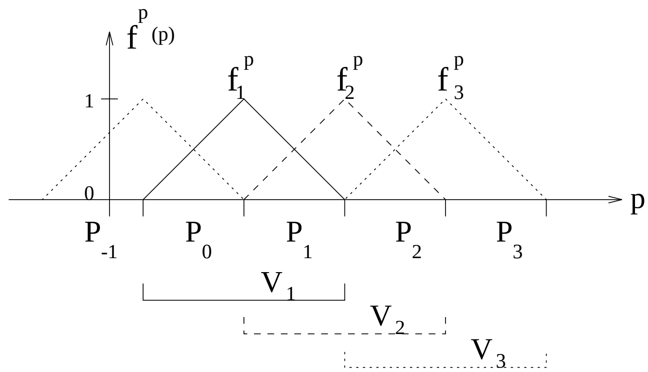

Figure 1: The profile of the basis function $\mathbf{f}_m^p(\mathbf{r}), m = 1, 2, 3, \cdots$.

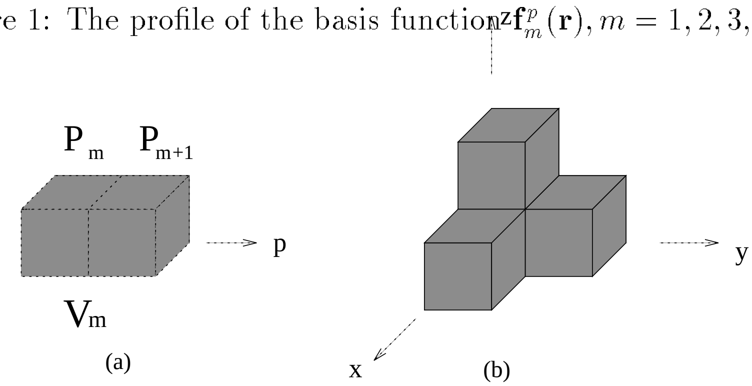

Figure 2: The supports of the face basis functions. (a) the support of $\mathbf{f}^p_{\mathbf{m}}(\mathbf{r})$; (b) the support of $\mathbf{f}_{\mathbf{m}}(\mathbf{r})$.

indices corresponding to the x, y, and z directions, respectively. For example, we will denote $\mathbf{f}_{ijk}$ by $\mathbf{f}_{\mathbf{m}}$ and P_{ijk} by $P_{\mathbf{m}}$.

Some remarks on the face basis functions:

1. Functions $\mathbf{f}^p_{\mathbf{m}}(\mathbf{r}), p = x, y, z$ are continuous in the direction p. Therefore the divergence of $\mathbf{f}_{\mathbf{m}}(\mathbf{r})$ is finite. The profile of $\mathbf{f}^p_{\mathbf{m}}(\mathbf{r})$ against coordinate p is shown in Figure 1.

2. The supports of $\mathbf{f}^p_{\mathbf{m}}(\mathbf{r})$ are overlapping in the direction p. This can be seen from Figures 2-(a) and 2-(b).

3. Functions $\mathbf{f}^p_{\mathbf{m}}(\mathbf{r})$ are piecewise linear in the direction p and piecewise constant in the other directions. As a result, the curl of $\mathbf{f}_{\mathbf{m}}(\mathbf{r})$ is not bounded.

4. If the sampling rate in the p^{th} direction is uniform, the functions $\mathbf{f}^p_{\mathbf{m}}(\mathbf{r})$ will be shift invariant in the p^{th} direction.

The first property discussed above eliminates the surface integration term due to integration by parts from Equation (12). As a consequence, the volume integration terms included in Equation (12) in each direction are four terms less than those when discontinuous basis functions are employed. For 3D vector fields, by using the rooftop functions to test the integral equation, twelve volume integration terms included in Equation (12) are removed and the effort of evaluating matrix $\bar{\mathbf{G}}$ is reduced by more than half.

However, the rooftop functions as bases for the total fields is not valid over the surface of the solution domain since it forces the field to be zero. The effect of this limitation on the terms which include the scattering parameter $\chi(\mathbf{r}')$ can be avoided since the function $\chi(\mathbf{r}')$ is zero outside the support of the scatterer, whereas the first term in Equation (10) includes $\epsilon(\mathbf{r}')$ instead of $\chi(\mathbf{r}')$. Hence, the effect of the rooftop function outside the solution domain need to be considered.

To ensure that the Galerkin's testing formulation is valid over the entire domain and to enforce the flux continuity boundary condition, we apply an extrapolation approach to approximate the field outside the surface of the solution domain. The face-based elements over the surface of the solution domain in the first term in Equation (10) are replaced by half rooftop function and half pulse function. In other words, the field $\mathbf{D}$ is approximated by rooftop bases inside the solution domain and one step zeroth order extrapolation outside the solution domain. As the size of the elements decreases, this approximation converges and the structure of the matrix $\bar{\mathbf{G}}$ retains a simple form.

3.2 Discrete Linear Kernels of the Testing Formulation

Applying the face-based elements described above into the testing formulation, Equation (10) — Equation (17), we can decompose the matrix $\bar{\mathbf{G}}$ into three independent parts: the scattering configuration, the kernels of the system, and the field values. The kernels are invariant with respect to the parameter of the scatterer and the incident fields. In doing so, we assume that the parameter of the scatterer, $\chi(\mathbf{r})$, can be approximated by a set of simple functions:

$$\chi(\mathbf{r}) \approx \sum \chi(\mathbf{m}) P_{\mathbf{m}}(\mathbf{r}). \tag{22}$$

Substituting the representations of $\chi(\mathbf{r})$ and the basis functions described above into Equation (12), and expanding the divergence of the equivalent current $\nabla' \cdot [\chi(\mathbf{r}')\mathbf{f_m}(\mathbf{r}')]$ by chain rule, we can decompose the matrix $\bar{\mathbf{G}}$, the elements of which are defined in Equation (15), into two parts, denoted by $\bar{\mathbf{G}}_1$ and $\bar{\mathbf{G}}_2$. Their elements can be written as:

$$g_{\mathbf{k},\mathbf{m}} = g_{1,\mathbf{k},\mathbf{m}} \chi(m) + g_{2,\mathbf{k},\mathbf{m}} \chi(\mathbf{m} + \vec{\Delta}) \tag{23}$$

where $\vec{\Delta}$ denotes the one step shift vector, and

$$\begin{aligned} g_{1,\mathbf{k},\mathbf{m}} &= -< \mathbf{f_k}, k_0^2 \int_{V_\mathbf{m}} g(\mathbf{r},\mathbf{r}')\boldsymbol{\phi}_\mathbf{m}(\mathbf{r}')d^3r' > \\ &\quad + < \nabla \cdot \mathbf{f_k}, \int_{V_\mathbf{m}} g(\mathbf{r},\mathbf{r}')\nabla' \cdot \boldsymbol{\phi}_\mathbf{m}(\mathbf{r}')d^3r' > \\ &\quad - < \nabla \cdot \mathbf{f_k}, \int_{s_\mathbf{m}} g(\mathbf{r},\mathbf{r}')\boldsymbol{\phi}_\mathbf{m}(\mathbf{r}') \cdot \hat{n} d^2r' >, \end{aligned} \tag{24}$$

and

$$\begin{aligned} g_{2,\mathbf{k},\mathbf{m}} &= -< \mathbf{f_k}, k_0^2 \int_{V_\mathbf{m}} g(\mathbf{r},\mathbf{r}')\boldsymbol{\psi}_{\mathbf{m}+\vec{\Delta}}(\mathbf{r}')d^3 > \\ &\quad + < \nabla \cdot \mathbf{f_k}, \int_{V_\mathbf{m}} g(\mathbf{r},\mathbf{r}')\nabla \cdot \boldsymbol{\psi}_{\mathbf{m}+\vec{\Delta}}(\mathbf{r}')d^3r' > \\ &\quad + < \nabla \cdot \mathbf{f_k}, \int_{s_\mathbf{m}} g(\mathbf{r},\mathbf{r}')\boldsymbol{\psi}_{\mathbf{m}+\vec{\Delta}}(\mathbf{r}') \cdot \hat{n} d^2r' > . \end{aligned} \tag{25}$$

The basis functions defined above have a property that they can be generated by shifting one basis function when their supports are of a uniform size. Therefore, we can represent them as:

$$\boldsymbol{\phi}_\mathbf{m}(\mathbf{r}) = \boldsymbol{\phi}_0(\mathbf{r} - \mathbf{r_m}), \quad \text{and} \quad \boldsymbol{\psi}_\mathbf{m}(\mathbf{r}) = \boldsymbol{\psi}_0(\mathbf{r} - \mathbf{r_m})$$

Substituting this relationship into Equation (24) and Equation (25), one can alter the domain of integrations over which the basis functions are supported to that where the support is fixed to one element, such as the 0^{th} element, and shift the Green's function to the corresponding elements. For example, one can write the integration involved in the testing formulation as:

$$< \mathbf{f_k}, k_0^2 \int_{V_\mathbf{m}} g(\mathbf{r},\mathbf{r}')\boldsymbol{\phi}_\mathbf{m}(\mathbf{r}')d^3r' > = < \mathbf{f}_0, k_0^2 \int_{V_0} g(\mathbf{r} - \mathbf{r}' + \mathbf{r_k} - \mathbf{r_m})\boldsymbol{\phi}_0(\mathbf{r}')d^3r' > \tag{26}$$

Similarly, the index $\mathbf{k}$ and $\mathbf{m}$ in all terms of $g_{1,\mathbf{k},\mathbf{m}}$ and $g_{2,\mathbf{k},\mathbf{m}}$ can be represented as the shift of $\mathbf{r_k} - \mathbf{r_m}$ in the Green's function;

$$< \nabla \cdot \mathbf{f_k}, \int_{V_\mathbf{m}} g(\mathbf{r},\mathbf{r}')\nabla' \cdot \boldsymbol{\psi}_{\mathbf{m}+\vec{\Delta}}(\mathbf{r}')d^3r' > = < \nabla \cdot \mathbf{f}_0, \int_{V_0} g(\mathbf{r} - \mathbf{r}' + \mathbf{r_k} - \mathbf{r_m} - \vec{\Delta})\nabla' \cdot \boldsymbol{\psi}_0(\mathbf{r}')d^3r' > \tag{27}$$

and

$$< \nabla \cdot \mathbf{f_k}, \int_{s_\mathbf{m}} g(\mathbf{r},\mathbf{r}')\boldsymbol{\phi}_\mathbf{m}(\mathbf{r}'))d^2s > = < \nabla \cdot \mathbf{f}_0, \int_{s_0} g(\mathbf{r} - \mathbf{r}' + \mathbf{r_k} - \mathbf{r_m})\boldsymbol{\phi}_0(\mathbf{r}'))d^2s > \tag{28}$$

Therefore, the matrix $\bar{\mathbf{G}}_1$ and $\bar{\mathbf{G}}_2$ can be represented by two 3×3 block Toeplitz matrices, respectively. In other words, their elements can be written as:

$$g_{1,\mathbf{k},\mathbf{m}} = g_{1,\mathbf{k}-\mathbf{m}} \quad \text{and} \quad g_{2,\mathbf{k},\mathbf{m}} = g_{2,\mathbf{k}-\mathbf{m}}$$

respectively. The 3D scattered field described in Equation (10) can be represented by the known discrete kernels. In doing so, we define the discrete kernels of the system:

$$h_{1q}(\mathbf{k}-\mathbf{m}) = < \mathbf{f}_0^q(\mathbf{r}), g(\mathbf{r}+\mathbf{r_k}-\mathbf{r_m}) * \boldsymbol{\phi}_0^q(\mathbf{r}) > \tag{29}$$

$$h_{2q}(\mathbf{k}-\mathbf{m}) = < \mathbf{f}_0^q(\mathbf{r}), g(\mathbf{r}+\mathbf{r_k}-\mathbf{r_m}) * \boldsymbol{\psi}_0^q(\mathbf{r}) > \tag{30}$$

$$I(\mathbf{k}-\mathbf{m}) = < P_0(\mathbf{r}), g(\mathbf{r}+\mathbf{r_k}-\mathbf{r_m}) * P_0(\mathbf{r}) > \tag{31}$$

$$J_q(\mathbf{k}-\mathbf{m}) = < P_0(\mathbf{r}), g(\mathbf{r}+\mathbf{r_k}-\mathbf{r_m}) * Q_0^q(\mathbf{r}) > \tag{32}$$

where $q = x, y, z$ represents the q^{th} component of the 3D vector field. $Q_0^q, q = x, y, z$ are 2D pulse functions with normal pointing to the $\hat{q}$ direction, respectively. Here, $*$ denotes the convolution operation in 3D.

Applying the shift invariant relationship described in Equations (26-28) to the testing formulation and substituting the kernels defined in Equations (29-32) into Equation (24) and Equation (25), we can represent the testing formulation (12) as 3D convolutions of these kernels with the discrete unknowns of the total field modulated with the parameters of the scatterers:

$$\begin{aligned} b^q(\mathbf{k}) \quad = \quad & \sum_{\mathbf{m}} a_{\mathbf{k},\mathbf{m}} d_{\mathbf{m}}^q - k_0^2 h_{1q}(\mathbf{k}) * t_1^q(\mathbf{k}) - k_0^2 z_q^{-1} h_{2q}(\mathbf{k}) * t_2^q(\mathbf{k}) \\ & + \sum_p [(1-z_q)(I(\mathbf{k}) - J_p(\mathbf{k}))] * t_1^p(\mathbf{k}) \\ & + \sum_p [(z_q - 1)(z_p^{-1} I(\mathbf{k}) - J_p(\mathbf{k}))] * t_2^p(\mathbf{k}) \end{aligned} \tag{33}$$

for $q = x, y, z$. where $(z_p, p = x, y, z)$ are one step forward shift operators with respect to the direction $\hat{p}$, z_p^{-1} is the corresponding backward shift operator, and

$$t_1^p(\mathbf{k}) = \chi(\mathbf{k}) d_{\mathbf{k}}^p \tag{34}$$

$$t_2^p(\mathbf{k}) = [z_p \chi(\mathbf{k})] d_{\mathbf{k}}^p \tag{35}$$

For brevity, the discrete formulation (33) can be written as a matrix form:

$$\mathbf{B}_q = \bar{\mathbf{A}}_q \cdot \mathbf{D}_q + \sum_p \bar{\mathbf{G}}_{1qp} \cdot \mathbf{T}_{1p} + \sum_p \bar{\mathbf{G}}_{2qp} \cdot \mathbf{T}_{2p} \tag{36}$$

$$\mathbf{T}_{1p} = \bar{\mathbf{\Lambda}}_{1p} \cdot \mathbf{D}_p \tag{37}$$

$$\mathbf{T}_{2p} = \bar{\mathbf{\Lambda}}_{2p} \cdot \mathbf{D}_p \tag{38}$$

where $\bar{\mathbf{G}}_{1qp}$ and $\bar{\mathbf{G}}_{2qp}$, for $p, q = x, y, z$, are Toeplitz matrices. They can be evaluated from the discrete kernels described above. And $\bar{\mathbf{\Lambda}}_{1p}$ and $\bar{\mathbf{\Lambda}}_{2p}$ are diagonal matrices with the parameters of the scatterers, $\chi(\mathbf{k})$ and $z_p\chi(\mathbf{k})$ as their diagonal elements, respectively. $\mathbf{D}_p$ is a vector that includes the unknown coefficients of the face-based elements with normal pointing to the $\hat{p}$ direction. $\mathbf{B}_q$ is the vector corresponding to the incident field in the $\hat{q}$ direction.

An interesting observation from Equation (33) is that solving the 3D scattering problems can be treated as solving the deconvolution problem of a discrete multi-input and multi-output system with known linear kernels. The equivalent inputs are the unknown total field $d^p, p = x, y, z$ which is modulated by χ, the parameter of the scatterer. The equivalent output is the known incident field b^p, for $p = x, y, z$. The discrete convolution in Equation (33) can be efficiently evaluated using FFT.

3.3 Properties of the Discrete Kernels

The basis functions employed here have the property that their supports are narrowly banded in the spatial domain. However, they have a rather wide bandwidth in the frequency domain. Therefore the complexity of evaluating these kernels in the spatial domain is of the order $2N + 1$ as opposed to the order $N \log_2 N$ in the frequency domain.

One also notes that the kernels are invariant with respect to the configuration of the scatterers, the magnitude, and the phase of the incident field. It only depends on the incident frequency. Therefore, for a given frequency, they can be evaluated in advance which simplifies the evaluation of 3D vector scattered field into the deconvolution of a discrete linear system. Based on the model of the scattered field described above, one can directly solve Equation (36) for the total field inside the scatterers. Meanwhile, the total field over the support of the scatterer is accurately modeled. Hence, it has significance in applications where electromagnetic waves inside the scatterer are considered.

3.4 BCG-FFT Iterative Algorithm

Since Equation (33) entails convolution and modulation, one can conveniently apply iterative type methods to solve for the total fields with respect to individual incident waves.

The continuous CG-FFT algorithms [8]-[10] have mainly two drawbacks. One is that it includes the basis functions inside the convolution. In other words, the convolution operation considered there is between the dyadic Green's function and the equivalent current. As a result, the dimension of the FFT has to be larger than the actual number of unknowns to achieve reasonable accuracy. The other shortcoming is that it is difficult to evaluate the conjugate transpose of the matrix. Consequently, the generalized CG residual algorithm has to be used to retain the computational complexity of order $N \log N$ per iteration. The condition number is squared and the convergence rate is decreased.

By using the discrete formulation derived above, the continuous convolution of the basis functions with the Green's function has been taken into account during the evaluation of the discrete kernels. Therefore the dimension of FFT for the discrete convolution in Equation (33) need not be increased. Furthermore, based on the discrete formulation, one can conveniently implement FFT for both matrix and conjugate transpose matrix multiplications. Therefore the biconjugate gradient approach can be used to solve for the field and retain the computational complexity as order $N \log N$. The BCG-FFT algorithm can be described as follows:

First we define the operations at the right hand side of Equation (36) as the operator $\mathcal{U}_q(\mathbf{D})$ which maps a field array $\mathbf{D}$ to an array with respect to the q^{th} component of the 3D field and is implemented using FFT:

$$\mathcal{U}_q(\mathbf{D}) = \bar{\mathbf{A}}_q \cdot \mathbf{D}_q + IFFT\{\sum_p \tilde{\bar{\mathbf{G}}}_{1qp}\tilde{\mathbf{T}}_{1p} + \sum_p \tilde{\bar{\mathbf{G}}}_{2qp}\tilde{\mathbf{T}}_{2p}\} \tag{39}$$

where $\tilde{\bar{\mathbf{G}}} = FFT\{\bar{\mathbf{G}}\}$ and $\tilde{\mathbf{T}} = FFT\{\mathbf{T}\}$. We note that the conjugate transpose of a Toeplitz matrix multiplying a vector results in a correlation relationship between the kernel and the vector. After some mathematical derivation, the multiplication between the conjugate transpose of the matrix and the vector $\mathbf{D}$ can be evaluated using FFT operations:

$$\mathcal{V}_q(\mathbf{D}) = \bar{\mathbf{A}}_q^H \cdot \mathbf{D}_q + \bar{\mathbf{\Lambda}}_{1p}^* IFFT\{\sum_p \tilde{\bar{\mathbf{G}}}_{1pq}\tilde{\mathbf{D}}_p^*\}^* + \mathbf{\Lambda}_{2p}^* IFFT\{\sum_p \tilde{\bar{\mathbf{G}}}_{2pq}\tilde{\mathbf{D}}_p^*\}^* \tag{40}$$

where $\bar{\mathbf{A}}^H$ denotes the conjugate transpose of $\bar{\mathbf{A}}$ and $*$ the complex conjugate.

Based on the generalized biconjugate gradient algorithm [21], the BCG-FFT algorithm for solving Equation (36) can be summarized as follows.

Starting with an initial guess $\mathbf{D}_0$ and compute:

$$\mathbf{R}_0 = \mathbf{B} - \mathcal{U}_q(\mathbf{D}_0) \tag{41}$$

$$\mathbf{P}_0 = \mathbf{R}_0^* \tag{42}$$

$$\mathbf{W}_0 = \mathbf{R}_0 \tag{43}$$

$$\mathbf{Q}_0 = \mathbf{P}_0 \tag{44}$$

Then evaluate

$$\alpha_i = \frac{< \mathbf{P}_i, \mathbf{R}_i >}{< \mathbf{Q}_i, \mathcal{U}(\mathbf{W}_i) >} \tag{45}$$

$$\mathbf{D}_{i+1} = \mathbf{D}_i + \alpha_i \mathbf{W}_i \quad (46)$$

$$\mathbf{R}_{i+1} = \mathbf{R}_i - \alpha_i \mathcal{U}(\mathbf{W}_i) \quad (47)$$

$$\mathbf{P}_{i+1} = \mathbf{P}_i - \alpha_i^* \mathcal{V}(\mathbf{W}_i) \quad (48)$$

$$\beta_i = \frac{< \mathbf{P}_{i+1}, \mathbf{R}_{i+1} >}{< \mathbf{P}_i, \mathbf{R}_i >} \quad (49)$$

$$\mathbf{W}_{i+1} = \mathbf{R}_{i+1} + \beta_i \mathbf{W}_i \quad (50)$$

$$\mathbf{Q}_{i+1} = \mathbf{P}_{i+1} + \beta_i^* \mathbf{Q}_i \quad (51)$$

for $i = 1, 2, \cdots$ until the convergence criterion is satisfied, where $\mathcal{U}(\mathbf{W}_i)$ and $\mathcal{V}(\mathbf{W}_i)$ are evaluated from Equation (39) and Equation (40) using FFT technique, respectively.

The above algorithm indicates that when FFT is used to evaluate $\mathcal{U}(\mathbf{W}_i)$ and $\mathcal{V}(\mathbf{W}_i)$, the computational complexity is of order $N \log N$ per iteration. One also observes that this algorithm can be implemented in a parallel form. It allows for the possibility of combining hardware with software to calculate the 3D scattered fields in real time.

4 Simulation Results

To analyze this discrete model, we have conducted numerical computation for the scattering of a plane wave from a dielectric sphere. The results are compared with Mie series solution. The criterion of the BCG convergence is $\frac{||\mathbf{R}_i||^2}{||\mathbf{R}_0||^2} < 10^{-6}$, where $||\mathbf{R}_i||$ denotes the norm of the residual of Equation (36) at the i^{th} iteration and $|R_0|$ is the norm of the initial residual.

In all simulations, we assume that the incident waves are plane wave with wavelength λ_0. The solution domain is a rectangle with center at (0,0,0). The bistatic RCS has the unit of per square wavelength dB which has the form [22]:

$$\sigma(\phi, \theta) = 10 \log_{10}(\sigma_\infty(\phi, \theta)/\lambda_0^2) \quad (52)$$

where

$$\sigma_\infty(\phi, \theta) = \lim_{R \to \infty} 4\pi R^2 \frac{||\mathbf{E}_s(\phi, \theta)||^2}{||\mathbf{E}_{inc}(\phi, \theta)||^2} \quad (53)$$

At the beginning of the simulation, we examine the electric field inside a layered lossy dielectric spherical object. The first layer has radius $a_1 = 0.075m$ and relative permittivity $\epsilon_{r,1} = 72.0 + j161.779$. The outer layer has radius $a_2 = 0.15m$ and relative permittivity $\epsilon_{r,2} = 7.5 + j8.9877$. The frequency of the incident wave is 100MHz which results in $ka_1 = 0.163$ and $ka_2 = 0.314$. The incident wave is polarized in the x direction and propagating in the z direction. The magnitudes of the source field computed using BCG-FFT algorithm and that

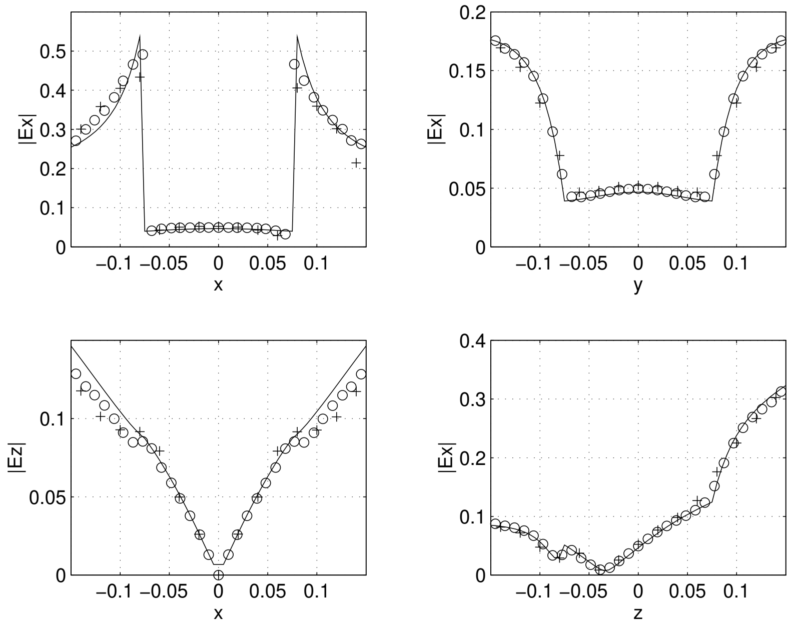

Figure 3: The magnitude of the components of the total electric field inside a layered lossy sphere; $a_1 = 0.075m$, $\epsilon_{r,1} = 72.0 + j161.779$, $a_2 = 0.15m$ and $\epsilon_{r,2} = 7.5 + j8.9877$; The solid line is from the Mie series solution; the BCG-FFT solution with grids $15 \times 15 \times 15$ is presented by the symbols $+$; the BCG-FFT solution with grids $30 \times 30 \times 30$ is presented by the symbols o;

from Mie series solution are shown in Figure 3. Two types of grid size are used for BCG-FFT to test the convergence of the program. One is $15 \times 15 \times 15$. Another is $31 \times 31 \times 31$. For the case of $15 \times 15 \times 15$ grid size, it takes 46 iterations for the BCG to converge and 22 seconds per iteration on the average on a SUN SPARC-10 WorkStation. When $31 \times 31 \times 31$ grids are used, the iteration number is the same and the CPU time for each iteration is 3.58 minutes on the average on the same computer.

Second, we consider a spherical dielectric scatterer where the ka ratio is one and $\epsilon_r = 4$. The scatterer is illuminated by a plane wave propagating in the z direction with $\hat{x}$ polarization. The bi-static RCS is plotted in Figure 4. The discrete grid is $12 \times 12 \times 12$ on a cube with side length $2a$. It takes 11 iterations for the BCG to converge and 1.5 minutes per iteration on the average on a SUN SPARC Station 2.

Figure 5 shows the robustness of this numerical model when the incident frequency is low. The permittivity of the scatterer are the same as shown in the first example. The incident frequency is 0.95 MHz which results in $ka_1 = 0.005$ and $ka_2 = 0.01$. The bi-static RCS is plotted in Figure 5. The grid is $15 \times 15 \times 15$. The total iteration number is 10. The CPU time for one iteration is 46 seconds on the average on a SUN SPARC-10 WorkStation.

In Figure 6, the size of the dielectric sphere is further enlarged to $a = 1.75\lambda_0$ so that

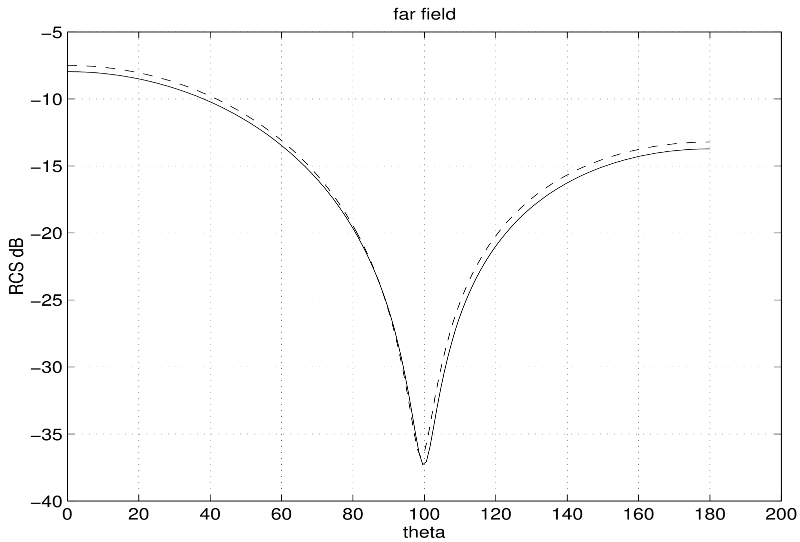

Figure 4: The Bi-RCS of a spherical scatterer. The solid line is from the Mie series solution; the numerical solution is presented by the dash line. $\epsilon_r = 4$, $ka = 1$, with $12 \times 12 \times 12$ grids.

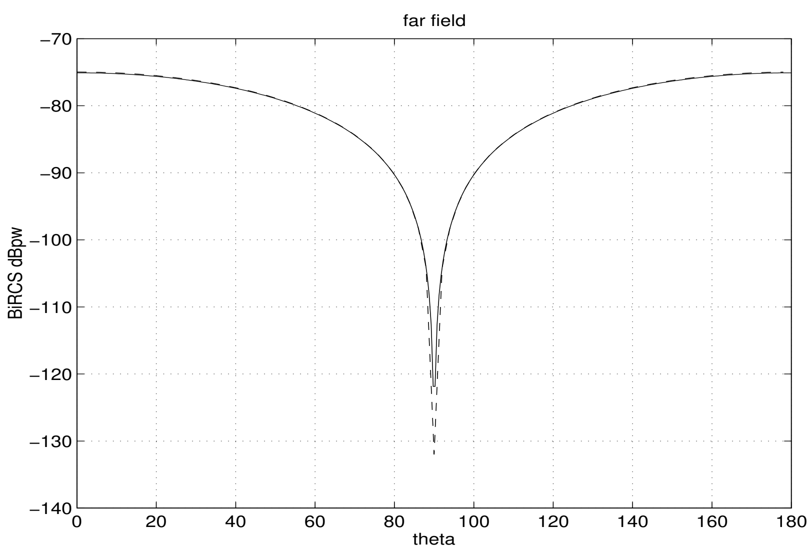

Figure 5: The Bi-RCS of a spherical scatterer. The solid line is from the Mie series solution; the dash line is the numerical solution; $\epsilon_{r,1} = 72.0 + j161.779$, $ka_1 = 0.01$, $\epsilon_{r,2} = 7.5 + j8.9877$, $ka_2 = 0.01$, with $15 \times 15 \times 15$ grids.

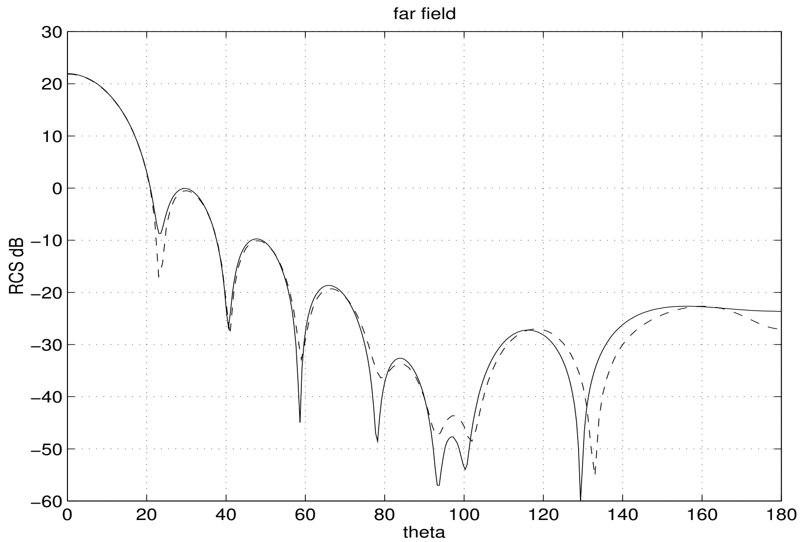

Figure 6: The Bi-RCS of a spherical scatterer. The solid line is from the Mie series solution; the dash line is the numerical solution. $\epsilon_r = 1.05$, $a = 1.75\lambda_0$, $ka = 11$, with $31 \times 31 \times 31$ grids.

$ka = 11$ and $\epsilon_r = 1.05$. The plane incident wave is in the negative z direction. Figure 6 shows the bi-static RCS. The sampling rate is 9 points per wave length. There are a total of 92,256 unknowns. The CPU time for one iteration is 4.8 minutes on a Convex machine. The total iteration number for convergence is 9.

Finally, we consider an inhomogeneous spherical dielectric object. The inhomogeneity contains three layers with respect to the center of the sphere as shown in Figure 7. The radius of the outside sphere is one wavelength. The operating frequency is 5.9MHz. The distribution of the permittivity from inside to outside is $\epsilon_{r,1} = 1.2$, $\epsilon_{r,2} = 2.0$, and $\epsilon_{r,3} = 2.4$, respectively. The results from BCG-FFT algorithm are compared with Mie series solution. In Figure 8, the magnitudes of the components of the electric field inside the inhomogeneous sphere are plotted. In Figure 9, the bistatic RCS from the spherically layered scatterer is presented. The grid size is $31 \times 31 \times 31$ with a total of 92,256 unknowns. The total iteration number of the BCG is 73. The CPU time per iteration is 3.35 minutes on the average on a SUN SPARC-10 WorkStation.

5 Conclusions

The discrete BCG-FFT algorithm for solving 3D EM scattering problem has been presented in this paper. In this method, the discrete biconjugate gradient approach is combined with

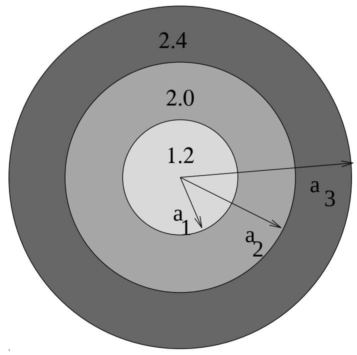

Figure 7: The distribution of the relative permittivity of the layered sphere; $a_1 = \frac{\lambda_0}{3}$, $a_2 = 2a_1$, and $a_3 = \lambda_0$ $\epsilon_{r,1} = 1.2$, $\epsilon_{r,2} = 2.0$, and $\epsilon_{r,3} = 2.4$

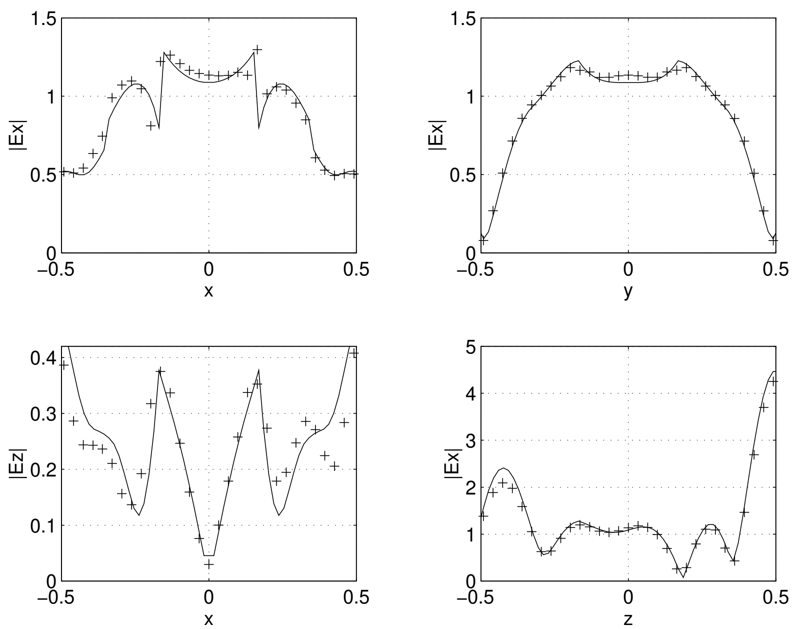

Figure 8: The magnitude of the components of the total electric field inside a layered sphere; $a_1 = 0.169m$, $\epsilon_{r,1} = 1.2$ $a_2 = 0.339m$, $\epsilon_{r,2} = 2.0$, and $a_3 = 0.508m$, $\epsilon_{r,3} = 2.4$; The solid line is from the Mie series solution; the BCG-FFT solution is presented by the symbols $+$. The grid size is $31 \times 31 \times 31$. The incident frequency results in $ka_3 = 6.28m$

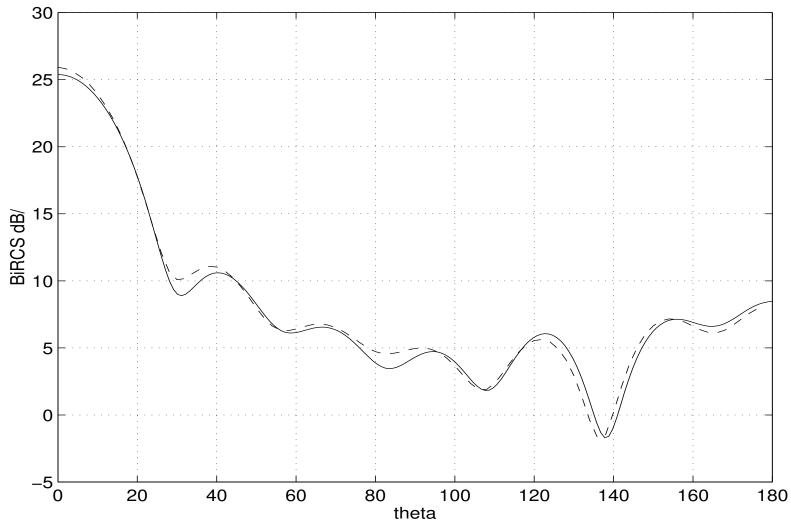

Figure 9: The Bi-RCS of a layered spherical scatterer. The solid line is from the Mie series solution; the dash line is the numerical solution. $a_1 = 0.169m$, $\epsilon_{r,1} = 1.2$ $a_2 = 0.339m$, $\epsilon_{r,2} = 2.0$, and $a_3 = 0.508m$, $\epsilon_{r,3} = 2.4$; with $31 \times 31 \times 31$ grids.

FFT technique to reduce the computational complexity per iteration from order N^2 to order $N \log_2 N$. The Galerkin's testing formulation has been represented accurately by a discrete linear system with multi-input and multi-output. Comparing with other CG-FFT methods as mentioned in the first section, this method avoids the singularity problem due to the Green's function and the limitation of the sampling rate of FFT.

The numerical simulation and the comparison of the results with those from theoretical solutions illustrate that the discrete model we have developed here provides a satisfactory solution with a sampling rate, at about ten samples per wavelength. The sampling rates and the scales with respect to the three coordinates on the Cartesian system can be adjusted according to different applications.

The numerical simulations also indicate that with large relative permittivity, the iteration number will be become large. An appropriate choice of pre-conditioner may be needed to speed up the convergence and enhance the robustness of the algorithm.

References

[1] P. M. Goggans, A. A. Kishk, and A. W. Glisson, "Electromagnetic scattering from objects composed of multiple homogeneous regions using a region-by-region solution," *IEEE Transactions On Antennas and Propagation*, vol. 42, no. 6, pp. 865–871, 1994.

[2] R. D. Graglia, P. L. E. Uslenghi, and R. S. Zich, "Moment method with isoparametric elements for three-dimensional anisotropic scatterers," *Proc. IEEE*, vol. 5, no. 77, pp. 750–760, 1989.

[3] J. M. Jarem, "Method-of-moments solution of a parallel-plate waveguide aperture system," *Journal of Applied Physics*, vol. 59, no. 5, pp. 3566–70, 1986.

[4] W. C. Chew, *Waves and Fields in Inhomogeneous Media.* New York: Van Nostrand Reinhold, 1990.

[5] G. Golub and J. M. Ortega, *Scientific Computing: an introduction with Parallel Computing.* New York: Academic Press, INC., 1993.

[6] M. R. Hestenes and E. Stiefel, "Methods and conjugate gradients for solving linear systems," *J. Res. Nat. Bur. Stand.*, vol. 49, pp. 409–436, 1952.

[7] W. C. Chew, C. C. Lu, and Y. M. Wang, "Efficient computation of three-dimensional scattering of vector electromagnetic waves," *J. Opt. Soc. Am. A*, vol. 11, no. 4, pp. 1–9, 1994. Forthcoming.

[8] M. F. Catedra, E. Gago, and L. Nuno, "A numerical scheme to obtain the rcs of three-dimensional bodies of size using the conjugate gradient method and the fast fourier transform," *IEEE Transactions On Antennas and Propagation*, vol. 5, no. 37, pp. 528 – 537, 1989.

[9] C. Y. Shen, K. J. Glover, M. I. Sancer, and A. D. Varvatsis, "The discrete fourier transform method of solving differential-integral equations in scattering theory," *IEEE Transactions On Antennas and Propagation*, vol. 8, no. 37, pp. 1032 – 1041, 1989.

[10] P. Zwamborn and P. M. van den Berg, "The three-dimensional weak form of the conjugate gradient FFT method for solving scattering problems," *IEEE Transactions On Microwave Theory and Techniques*, vol. 9, no. 40, pp. 1757 – 1766, 1992.

[11] Z. S. B and Y. Leviatan, "On the use of wavelet expansions in the methods of moments," *IEEE Transactions On Antennas and Propagation*, vol. 5, no. 41, pp. 610–619, 1993.

[12] R. L. Wagner, G. P. Otto, and W. C. Chew, "Fast waveguide mode computation using wavelet-like basis functions," *IEEE Microwave and Guided Wave Letters*, vol. 7, no. 3, pp. 208–210, 1993.

[13] D. T. Borup and O. P. Gandhi, "Fast-Fourier transform method for calculation of SAR distributions in finely discretized inhomogeneous models of biological bodies," *IEEE Transactions On Microwave Theory and Techniques*, vol. 32, no. 4, 1984.

[14] M. F. Catedra, "Solution to some electromagnetic problems using fast Fouier transform with conjugate gradient method," *Electron Letter*, vol. 22, no. 9, pp. 1049–1051, 1986.

[15] A. F. Peterson and R. Mittra, "Method of conjugate gradient for the numerical solution of large-body electromagnetic scattering problems," *J. Opt. Soc. Am*, vol. 2, no. 6, pp. 971–977, 1985.

[16] T. K. Sarkar, E. Arvas, and S. M. Rao, "Application of FFT and the conjugate gradient method for the solution of electromagnetic radiation from electrically large and small conducting bodies," *IEEE Transactions On Antennas and Propagation*, vol. 34, pp. 635–639, 1986.

[17] M. F. Catedra and J. G. Cuevas, "A scheme to analyze conducting plates of resonant size using the conjugate gradient method and the fast fourier transform," *IEEE Transactions On Antennas and Propagation*, vol. 36, no. 12, pp. 1744–1752, 1988.

[18] Q. H. Liu and W. C. Chew, "Application of the conjugate gradient fast Fourier Hankel transfer method with an improved fast Hankel transform algorithm," *Radio Science*, vol. 9, no. 4, pp. 1009–1022, 1994.

[19] D. F. Elliot and K. R. Rao, *Fast Transforms, Algorithms, Analyses, Applications.* New York: Academic, 1982.

[20] J. G. Proakis and D. G. Manolakis, *Digital Signal Processing: Principles, Algorithm, and Applications.* New York: Macmillan Publishing company, 2 ed., 1992.

[21] T. K. Sarkar, "On the application of the generalized biconjugate gradient method," *J. of Electromagnetic Waves and Application*, vol. 1, no. 3, pp. 223–242, 1987.

[22] C. A. Balanis, *Advanced Engineering Electromagnetics.* New York: Wiley, 1989.